ELSEVIER

Solid State Nuclear Magnetic Resonance 8 (1997) 1–16

SOLID STATE
Nuclear Magnetic
Resonance

Multiple-quantum magic-angle spinning and dynamic-angle spinning NMR spectroscopy of quadrupolar nuclei

S.H. Wang [a], Z. Xu [b], J.H. Baltisberger [c], L.M. Bull [d], J.F. Stebbins [b], A. Pines [a,*]

[a] *Materials Sciences Division, Lawrence Berkeley Laboratory and Department of Chemistry, University of California, Berkeley, CA 94720, USA*
[b] *Department of Geological and Environmental Sciences, Stanford University, Stanford, CA 94305, USA*
[c] *Department of Chemistry, Berea College, Berea, KY 40404, USA*
[d] *Materials Research Laboratory, University of California, Santa Barbara, CA 93106, USA*

Received 12 July 1996; accepted 13 September 1996

Abstract

Several aspects of the Multiple-Quantum Magic-Angle Spinning (MQMAS) technique (L. Frydman and J.S. Harwood, J. Am. Chem. Soc., 117 (1995) 5367) are compared with Dynamic-Angle Spinning (DAS). Examples of MQMAS spectra are shown for $I = 3/2$ nuclei with C_Q up to 3.6 MHz, and for ^{27}Al ($I = 5/2$) with C_Q up to 10 MHz. The MQMAS linewidth is largely independent of the magnitude of the homonuclear dipolar interaction, while the spinning sideband manifold is similar to that observed in DAS experiments. MQMAS is technically simple and routinely useful for studying nuclei with short spin–lattice relaxation times, but care must be taken in its use for quantitative studies as the excitation of the triple-quantum coherence is not uniform. In this regard, MQMAS is most useful for samples with small quadrupolar coupling constants. In the specific case of ^{17}O, DAS would give spectra with excellent resolution in comparison to MQMAS. The different advantages of DAS and MQMAS make them useful complementary techniques in many cases.

Two additional methods are also presented for extracting the chemical shift anisotropy (CSA) directly for quadrupolar nuclei using the multiple-quantum scheme. © 1997 Elsevier Science B.V. All rights reserved.

Keywords: Chemical shift anisotropy; Dynamic-angle spinning; Multiple-quantum magic-angle spinning; Quadrupolar nuclei; Tensor orientation

1. Introduction

High-resolution solid-state NMR spectra for spin 1/2 nuclei are now readily attainable since Magic-Angle Spinning (MAS) [1–3] averages away anisotropic interactions including chemical shifts and heteronuclear dipolar couplings. In contrast, quadrupolar nuclei in solids usually experience a large quadrupolar interaction, which can not be totally removed by MAS [4,5]. For half-integer quadrupolar nuclei, interest has largely been focused on the central ($1/2 \leftrightarrow -1/2$) transition, because it is not affected by the first-order quadrupolar interaction. However, the MAS spectra are still shifted and broadened by the second-order quadrupolar interaction, which limits the resolution for many important nuclei [4,5].

---

[*] Corresponding author.

0926-2040/97/$17.00 © 1997 Elsevier Science B.V. All rights reserved.
PII S0926-2040(96)01277-5

Techniques proposed for overcoming this resolution problem include DOuble Rotation (DOR) [6–8] in which the sample is simultaneously spun about two axes, and Dynamic-Angle Spinning (DAS) [8–10], in which the sample is spun sequentially about two axes giving a 2D NMR spectrum that correlates isotropic and anisotropic information characteristic of the distinct sites. DAS and DOR have been successfully used to study nuclei such as ^{17}O [11,12], ^{23}Na, ^{27}Al [13], and ^{87}Rb [14]. Recently, Frydman and coworkers [15,16] introduced an alternative approach (Multiple-Quantum Magic-Angle Spinning, MQMAS) that utilizes the multiple-quantum coherence [17,18] to achieve high-resolution. The experiment involves sample spinning around only the magic angle, which is technically much simpler than DAS or DOR and makes it a very promising technique for the study of quadrupolar nuclei.

In this paper, we address several complimentary aspects of MQMAS and DAS. Issues such as excitation, linewidth, resolution, sideband pattern and the effect of other interactions including CSA and dipolar coupling are discussed. It is shown that CSA parameters can be directly extracted from the simulation of the MQMAS spectrum when the magnitude of the CSA is comparable to that of the second-order quadrupolar interaction in the single-quantum spectrum. If, on the other hand, the CSA is moderate, a MQVAS (Multiple-Quantum Variable-Angle Spinning) method can be used to provide direct CSA information.

2. Theory

This section provides a brief description of the theoretical background related to the current paper. For a quadrupolar system, the relevant Hamiltonian contains the following term:

$$H = H_Z + H_Q + H_{CS} + H_D \tag{1}$$

where H_Z, H_Q, H_{CS} and H_D represent the Zeeman, quadrupolar, chemical shift and dipolar interactions, respectively. The Zeeman interaction is usually so large that all the other interactions can be treated as perturbations.

As a starting point, consider only the Zeeman and quadrupolar Hamiltonians H_Z and H_Q. Application of the first-order perturbation theory to this problem gives the resonance frequency correction due to H_Q:

$$\omega^{1Q}_{m\leftrightarrow n} = \frac{3C_Q}{2\sqrt{6}\,I(2I-1)}(m^2-n^2)\,A^Q_{2,0}(\alpha,\beta) \tag{2}$$

In Eq. (2), $m \leftrightarrow n$ designates a transition between nuclear spin states m and n, $C_Q = e^2qQ/h$ is the quadrupolar coupling constant and I is the nuclear spin quantum number. $A^Q_{2,0}$is a function of the Euler angles α and β between the molecular frame and the laboratory frame. It is these two angles that characterize the spatial dependence of the quadrupolar interaction.

According to Eq. (2), the $m \leftrightarrow -m$ transitions are not affected by the first-order correction. Applying the second-order perturbation calculation [15] to these transitions gives

$$\begin{aligned}\omega^{2Q}_{m\leftrightarrow -m}(\alpha,\beta,\theta) &= C_0(I,m)\,\omega^{2Q}_{\mathrm{iso}} + C_1(I,m)\,A^Q_2(\alpha,\beta)\,P_2(\cos\theta)\\ &\quad + C_2(I,m)\,A^Q_4(\alpha,\beta)\,P_4(\cos\theta)\end{aligned} \tag{3}$$

as the time-independent part. In Eq. (3), α and β are Euler angles between the molecular and the rotor frames, and A^Q_2 and A^Q_4 are the orientation-dependent terms that broaden the spectra and need to be averaged away to achieve high resolution. P_2 and P_4 are the second- and fourth-order Legendre polynomials as a function of spinning angle θ. C_0, C_1 and C_2 are constants dependent on the observed transition and the spin quantum number I; they are listed in Table 1.

When the chemical shift Hamiltonian is considered, the first-order perturbation calculation gives

$$\omega^{CS}_{m\leftrightarrow -m}(\alpha,\beta,\theta) = 2m\gamma B\big(\delta_{\mathrm{iso}} + A^{CS}_2(\alpha,\beta)\,P_2(\cos\theta)\big) \tag{4}$$

where A^{CS}_2 is the orientation-dependent term and similar definitions of α, β and θ have been used. It is evident from Eq. (4) that the chemical-shift dispersion in an m-quantum spectrum is magnified by a factor of m in comparison with such a dispersion in a single-quantum spectrum. This dispersion could result in higher resolution spectra and provide a means of measuring the CSA if it is too small to be resolved in a single-quantum spectrum. Examples will be given in the later sections.

Table 1
Coefficients in the second-order quadrupolar Hamiltonian (C_0, C_1, C_2) (Eq. (3)), the ratios between the two-separated t_1 periods (k) (Eq. (6)) and the scaling factors (k_1, k_2) (Eq. (9)) for the MQMAS isotropic frequency

I	m	C_0	C_1	C_2	k	k_1	k_2
3/2	1/2	3	−12	−27	–	–	–
3/2	3/2	−9	0	21	7/9	17/8	−5/4
5/2	1/2	8	−32	−72	–	–	–
5/2	3/2	6	−60	−114	19/12	−17/31	10/31
5/2	5/2	−50	20	150	25/12	61/37	−50/37
7/2	1/2	15	-60	−135	–	–	–
7/2	3/2	27	−144	−303	101/45	−17/73	10/73
7/2	5/2	−15	−120	−165	11/9	−4/5	1
7/2	7/2	−147	168	483	161/45	148/103	−140/103
9/2	1/2	24	−96	−216	–	–	–
9/2	3/2	54	−252	−546	91/36	−17/127	10/127
9/2	5/2	30	−300	−570	95/36	−13/131	50/131
9/2	7/2	−84	−168	−84	7/18	−47/25	14/5
9/2	9/2	−324	216	1116	31/6	79/55	−50/37

It is worth noting that normal MAS is not enough to average away the anisotropies in Eq. (3) since the P_4 term still broadens the spectra. One way to remove the full anisotropy is to make the spinning angle time-dependent [6–10]. In a DAS experiment, the sample is spun sequentially around two angles fulfilling the following conditions:

$$C_1(I,1/2)P_2(\cos\theta_1) = kC_1(I,1/2)P_2(\cos\theta_2) \tag{5a}$$

$$C_2(I,1/2)P_4(\cos\theta_1) = kC_2(I,1/2)P_4(\cos\theta_2) \tag{5b}$$

where (θ_1, θ_2) is a DAS angle pair and k is between 0.8 and 5 ($k = |P_2(\cos\theta_1)/P_2(\cos\theta_2)|$). One can view this DAS experiment as a technique which manipulates P_2 and P_4 in Eqs. (3) and (4) to achieve high resolution, since the C_1 or C_2 term in Eqs. (5a) and (5b) actually cancelled. For the same purpose, the novel MQMAS experiment manipulates P_2, P_4 and C_1, C_2 simultaneously; it removes the A_2^{CS} and A_2^{Q} terms by sample spinning at the magic angle (where P_2 is zero), and eliminates the A_4^{Q} term by a correlation of the single and triple-quantum coherences. In this MQMAS case, k is defined by the equation:

$$C_2(I,3/2)P_4(\cos\theta) = kC_2(I,1/2)P_4(\cos\theta) \tag{6}$$

Notice the similar cancellation of the P_4 factor, which results in $k = |C_2(I,3/2)/C_2(I,1/2)|$. k values for different spins are also listed in Table 1.

One significant point here is that a specific P_4 or P_2 term *can* be removed by *correlation* even if the sample is not spinning at the angle with P_4 or P_2 equal to zero. In this regard, if we spin the sample at 70.12° or 30.56° ($P_4(\cos\theta) = 0$), and use the correlation scheme to remove A_2^{Q} (in MQMAS, A_4^{Q} is removed by correlation), the only anisotropic term left is A_2^{CS}, which gives the CSA parameters directly. This experiment is particularly easy to implement for spin 3/2 nuclei since the $3/2 \leftrightarrow -3/2$ transition does not have the A_2^{Q} term [19]:

$$\omega^{CS}_{3/2\leftrightarrow -3/2}(\alpha,\beta,\theta) = 3\gamma B\left(\delta_{iso} + A_2^{CS}(\alpha,\beta)P_2(\cos\theta)\right) \tag{7a}$$

$$\omega^{2Q}_{3/2\leftrightarrow -3/2}(\alpha,\beta,\theta) = C_0(3/2,3/2)\,\omega^{2Q}_{iso} + C_2(3/2,3/2)A_4^{Q}(\alpha,\beta)P_4(\cos\theta) \tag{7b}$$

Spinning the sample at 70.12° or 30.56° leaves A_2^{CS} as the major term [19] that broadens the triple-quantum spectrum. Since multiple quantum signals can not be detected directly, a 2D experiment is needed which gives a spectrum with a triple-quantum CSA dimension and a single-quantum Variable-Angle Spinning (VAS) dimension. This technique is referred to as MQVAS (Multiple-Quantum Variable-Angle Spinning).

3. Experimental

All of the inorganic compounds used in the experiment were obtained from commercial sources, typically with a stated purity of at least 98%. The anorthite and ^{17}O-enriched stilbite were made at Stanford University and characterized by XRD and ^{29}Si NMR. Preparation details and more extensive spectral analysis of these samples are found elsewhere [20].

The ^{23}Na, ^{87}Rb, ^{17}O and ^{45}Sc experiments were performed at either 9.4 T or 11.7 T using a home-built 5-mm DAS probe [21]. The spinning axis was initially set to 54.74° by maximizing the observed sideband intensity using KBr (^{81}Br) or d-HMB (^{2}H) as standards. The ^{27}Al spectra were collected using a Doty Scientific 5-mm high-speed MAS probe. Spinning speeds greater than 7.5 kHz were used in all experiments except for the one designed to give the intense $^{23}Na_2C_2O_4$ sideband pattern. The RF power level in the DAS experiments was set to ensure selective excitation of the central transition, and a typical 90° pulse length was ~ 7 μs. In the MQMAS experiments, high power was used to achieve efficient excitation with a typical 90° pulse length of ~ 2 μs.

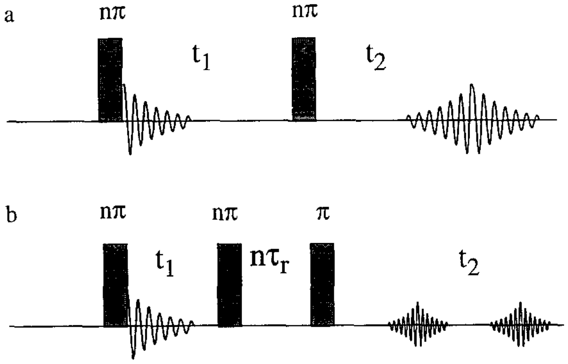

Fig. 1. Pulse sequences used in MQMAS and MQVAS experiments: (a) simple two-pulse sequence; (b) three-pulse shifted-echo sequence.

The shifted-echo DAS sequence ($\pi/2$–t_1–$\pi/2$–hop–$\pi/2$–tau–π–acq.) used in our experiments is described elsewhere [22]. The echoes were typically shifted out by many milliseconds (if possible) to achieve high sensitivity and an undistorted signal. Similarly, a shifted-echo MQMAS sequence [23] was usually used for the MQMAS experiments (Fig. 1(b)). However, if the sensitivity was a problem due to T_2 decay under echo conditions, the simple two-pulse MQMAS sequence [16,23,24] was used (Fig. 1(a)). (It is worth pointing out that maximum multiple-quantum excitation and conversion efficiency is not necessarily achieved by these sequences [25].) The data were processed according to the method suggested by Grandinetti [22,23].

4. Results and discussion

4.1. Feasibility of DAS and MQMAS

MQMAS spectra of ^{23}Na ($I = 3/2$), ^{87}Rb ($I = 3/2$), ^{27}Al ($I = 5/2$), ^{17}O ($I = 5/2$) and ^{45}Sc ($I = 7/2$) in some model compounds are shown in Fig. 2. The typical recycle delay varies between 0.5 s and 1 s for different samples, resulting in an acquisition time no longer than 12 h. This suggests that a MQMAS spectrum can be acquired in a reasonable time for these nuclei (also for ^{11}B, $I = 3/2$) when the T_1 of the sample is not very long. The quadrupolar coupling constants (C_Q) are 3.6 MHz for ^{87}Rb in $RbClO_4$ [14], 2.4 MHz for ^{23}Na in $Na_2C_2O_4$ [16], about 5 MHz for the ^{45}Sc sites in $Li_3Sc_2(PO_4)_3$, 2.8–8.4 MHz for ^{27}Al sites in anorthite [20,26] and 3.4 and 4.8 MHz for the two types of site in ^{17}O-labeled stilbite. The MAS dimension of these spectra usually shows well defined MAS powder patterns, suggesting a relatively even excitation of the triple-quantum transition [16].

The single-hop DAS spectra for the above ^{87}Rb, ^{23}Na and ^{17}O samples were also obtained. However, acquisition of the ^{11}B, ^{27}Al and ^{45}Sc DAS spectra was far less successful because of the short T_1s. Typically, 30–50 ms are needed to flip the spinning angle in a DAS experiment which means it can only be applied to samples with T_1 longer than 100–150 ms. Another limiting factor for DAS is the homonuclear dipolar coupling, which creates coher-

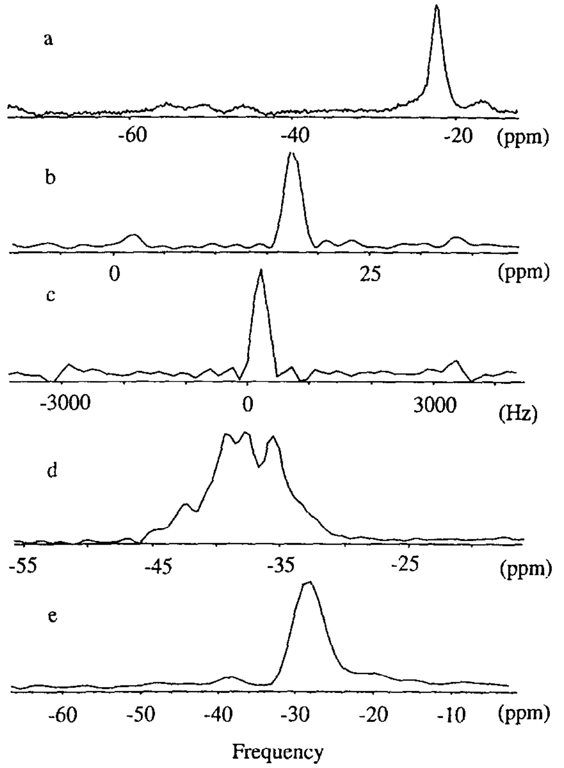

Fig. 2. MQMAS spectra of (a) $^{87}RbClO_4$, (b) $^{23}Na_2C_2O_4$, (c) ^{45}Sc in $Li_3Sc_2(PO_4)_3$, (d) ^{27}Al in anorthite, (e) ^{17}O in stilbite. Spectra (a), (b), and (d) were taken at 11.7 T whereas the other two were taken at 9.4 T. Frequencies are referenced to 1 M $RbNO_3$ for ^{87}Rb, 1 M NaCl for ^{23}Na, 1 M $Al(NO_3)_3$ for ^{27}Al, and H_2O for ^{17}O. The ^{45}Sc spectral scale is shown in Hz, as a chemical-shift standard was not available. Spectrum (d) is a slice taken along the isotropic dimension, which has better resolution than the isotropic projection. In a 2D contour-plot, five of the eight ^{27}Al sites in that system can be differentiated [20]. Two types of ^{17}O site exist in stilbite, but only one peak can be seen in (e).

ences that may not be restored following axis reorientation [27]. There is no such limitation for MQMAS because a hopping period is not necessary between the two correlation evolution periods.

The major limiting factor for MQMAS is the magnitude of the quadrupolar interaction. Since the triple-quantum transition is forbidden to first-order, the MQMAS experiment is currently limited to sites with C_Q less than 4 MHz for spin 3/2 nuclei [16]. As a comparison, a C_Q of up to 6.5 MHz for $I = 3/2$ nuclei does not lead to extra experimental difficulties for DAS [14]. In the extreme, Grandinetti et al. have obtained a ^{71}Ga ($I = 3/2$) DAS spectrum for β-Ga_2O_3 with a C_Q of $\sim$ 12 MHz [28].

It has been shown that the excitation efficiency of the triple-quantum coherence is determined by ν_Q/ν_{rf} [16–18,25]. To achieve maximum excitation efficiency, the highest power level is usually used. When the RF strength is fixed, the quantity that determines the excitation efficiency is ν_Q which is defined as

$$\nu_Q = C_Q/2I(2I-1) \tag{8}$$

and smaller ν_Q usually means better excitation unless ν_Q is vanishingly small. It is thus not surprising to see the efficient excitation for ^{27}Al (Fig. 1(d), anorthite, with C_Q's up to 8.4 MHz), but the inferior excitation for ^{87}Rb (Fig. 1(a), $RbClO_4$, $C_Q =$ 3.6 MHz). The smaller scaling factor for $I > 3/2$ nuclei suggests that the observation of C_Q up to 9 MHz for ^{27}Al is possible, based on the relatively efficient excitation of the triple-quantum coherence for ^{23}Na (e.g. $Na_2C_2O_4$, $I = 3/2$, $C_Q = 2.4$ MHz). This is actually demonstrated by our experiment on kyanite [20], which has ^{27}Al site with C_Q up to 10.0 MHz. The fact that the excitation scheme in Fig. 1 is relatively efficient for spin 5/2 nuclei is important because C_Q's for ^{27}Al and ^{17}O are smaller than 10 MHz in a lot of commonly used technological materials [26,29]. However, some care must be taken in the use of this technique for the study of site quantification.

4.2. Linewidth

The DAS and MQMAS linewidths (full width at half maximum) of some model compounds are compared in Table 2. Also shown in this table are the linewidth data from MAS and Hahn-echo experiment (T_2-linewidth). In addition, the DAS linewidths for ^{11}B in D_3BO_3 [27], ^{27}Al in $LiAlSi_4O_{10}$ [30] and ^{17}O in diopside [11] are also included.

The DAS linewidth increases from about 200 Hz for ^{87}Rb to 1.2 kHz for ^{27}Al, consistent with the increasing homonuclear dipolar coupling as shown in Table 2. The MQMAS linewidth, on the other hand, is largely nucleus-independent, spanning the range between 170 Hz and 270 Hz. While the DAS and MQMAS lines are usually an order of magnitude narrower than the MAS lines, they are an order of

Table 2
Comparison of the DAS, MQMAS, echo, and MAS linewidths for some model compounds

Nucleus/compound	DAS linewidth (Hz) [a]	MQMAS linewidth (Hz) [a]	Echo linewidth (Hz) [a]	MAS linewidth (Hz) [b]
$^{87}RbNO_3$ [c]	160	180	10	~ 2500
$^{87}RbClO_4$	250	270	10	~ 5000
$^{23}Na_2C_2O_4$	500	260	25	~ 3500
$D_3^{11}BO_3$	1100 [e]	–	–	~ 4500
^{27}Al Kyanite	–	170	30	~ 7300
^{27}Al $LiAlSi_4O_{10}$	1200 [f]	–	–	~ 4200 [f]
^{17}O Diopside	120 [f]	–	–	~ 3800 [g]
^{17}O Stiblite [d]	600	270	30	~ 4500

[a] Full width at half magnitude.[b] Full spectral range covered by the MAS spectra. Notice that many sites may exist in some of the samples.[c] Linewidths of the site with $C_Q = 1.72\,\mathrm{MHz}$, $\eta_Q = 0.5$, $\delta_{iso} = -31.3\,\mathrm{ppm}$.[d] There is a distribution of the ^{17}O sites in stilbite.[e] Ref. [26].[f] Ref. [29].[g] Ref. [11].

magnitude broader than the echo linewidth. This is not a surprise as magnetic field inhomogeneity as well as inhomogeneous broadenings are all refocused by an echo sequence, leaving only the intrinsic T_2 relaxation under MAS. To understand completely why the MQMAS lines are so much wider than the

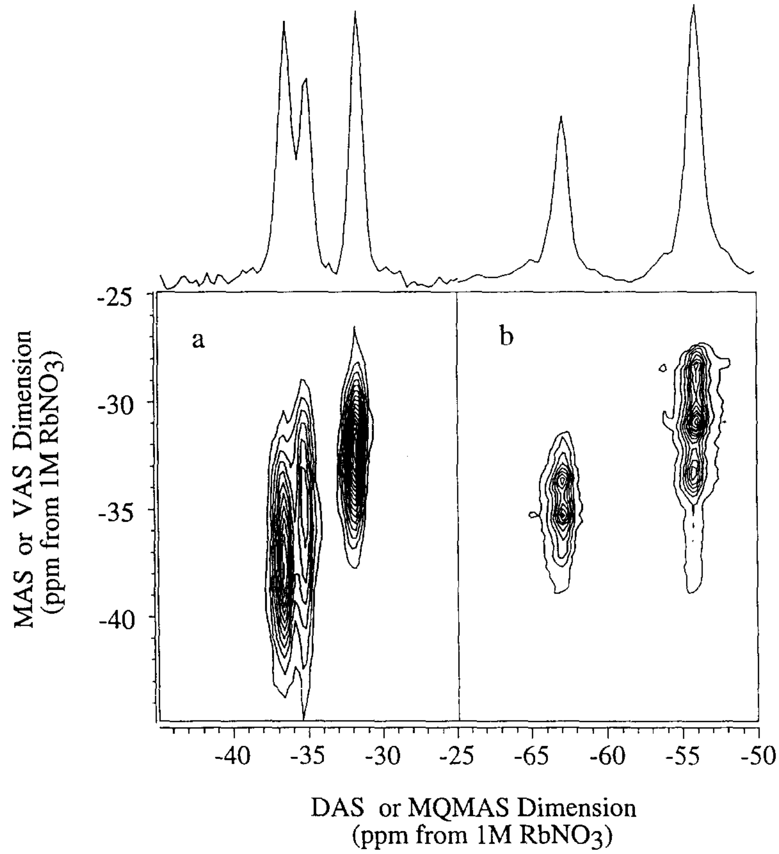

Fig. 3. 11.7 T DAS (a) and MQMAS (b) spectra of $^{87}RbNO_3$. The contour lines are drawn from a level of 5% to a level of 100% with an increment of 5%. Note that the two low-frequency peaks in the DAS spectrum appear on the high-frequency side of the MQMAS spectrum.

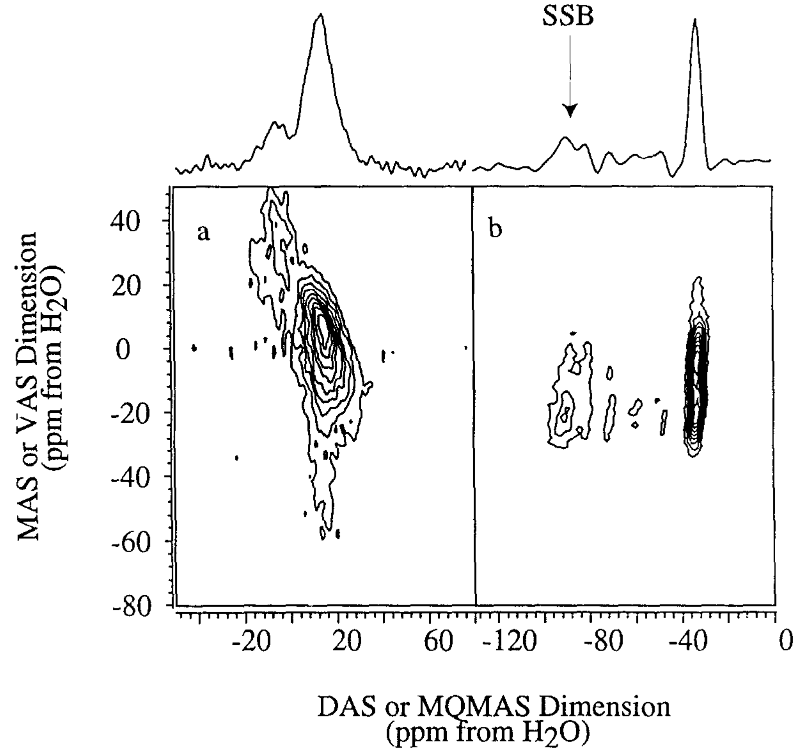

Fig. 4. 9.4 T DAS (a) and MQMAS (b) spectra of ^{17}O-labeled stilbite. The contour lines are drawn from a level of 5% to a level of 100% with an increment of 5%. Two DAS peaks are discernible, with only one peak discernible in the MQMAS spectrum (the left-hand side intensity is from spectral distortion and sideband).

echo lines requires more detailed and careful experiments to evaluate the contribution of each broadening mechanism.

The DAS linewidth can be related to the magnitude of the homonuclear dipolar interaction in the system [27]. The bilinear terms in the density matrix arising from the dipolar Hamiltonian can not be retained through a DAS angle change. Thus the dipolar Hamiltonian acts purely as a relaxation superoperator and it is not refocused at the DAS echo maximum. The independence of the MQMAS linewidth on the nucleus of interest suggests that homonuclear dipolar coupling is not a crucial factor for the implementation of the MQMAS experiment, a major advantage over DAS.

4.3. Resolution

The observed DAS and MQMAS shifts (in ppm) are given by:

$$\delta_{\mathrm{obs}} = k_1 \delta_{\mathrm{iso}} - k_2 \delta_{\mathrm{iso}}^{2Q} \tag{9}$$

where

$$\delta_{\mathrm{iso}}^{2Q} = \frac{3 \times 10^6}{10} \frac{C_Q^2(I(I+1) - 3/4)}{\omega_0^2 [2I(2I-1)]^2} (1 + \eta^2/3) \tag{10}$$

is the second-order quadrupolar shift [33]. The scaling factors k_1 and k_2 are different for DAS ($k_1 = k_2 = 1$) and MQMAS (Table 1), making the resolution of the spectrum dependent not only on δ_{iso} and $\delta_{\mathrm{iso}}^{2Q}$, but also on k_1 and k_2. Some general conclusions about resolution can be drawn but for specific samples; care must be taken in spectral interpretation.

Eq. (9) indicates that two chemically different sites having the same quadrupolar coupling constants will have a frequency separation proportional to k_1. If $|k_1|$ is greater than 1.0, better resolution is expected for MQMAS; if, on the other hand, $|k_1|$ is smaller than 1.0, DAS will give better resolution. The factor k_2 in Eq. (9) has a similar effect on resolution. In the case of $I = 3/2$ nuclei, MQMAS gives better resolution than DAS according to Table 1, and the opposite is true for $I > 3/2$ nuclei. For $I = 3/2$ nuclei, the enhanced resolution of MQMAS over DAS is readily seen in Fig. 3 where the separation of the two MQMAS peaks in $RbNO_3$ (9 ppm) is twice that in the DAS spectrum (5 ppm). Discussion about the overlapping of the two high-field DAS peaks in the MQMAS spectrum is provided in Section 4.4. For $I = 5/2$ nuclei, an example is given in Fig. 4, which is an ^{17}O stilbite spectrum taken at 9.4 T. In this case, DAS gives two partially resolved peaks, whereas only one peak is observed in the MQMAS spectrum. Similar resolution limitation was also encountered for ^{45}Sc ($I = 7/2$).

MQMAS is a promising technique for the study of ^{27}Al ($I = 5/2$) because MAS spectra for ^{27}Al are usually too broad to take advantage of the improved spectral dispersion. The moderate coupling constants for ^{27}Al in most materials [26,29] make it very suitable for MQMAS studies [20].

The decreased resolution for $I > 3/2$ nuclei in the 3QMAS spectrum can be overcome by correlating the $2I$-quantum coherence with the single-quantum coherence [31]. This is demonstrated in Fig. 5, where the 5QMAS ^{27}Al spectrum of goosecreekite ($CaAl_2Si_6O_{16} \cdot 5H_2O$) clearly shows two different Al sites [32], resolving the structural controversy of this zeolite. The five-quantum coherence is easily generated for samples with small quadrupolar coupling constants. The question of excitation for large coupling constants is a future problem in the utilization of these higher-order multiple-quantum experiments.

4.4. Combined effect of chemical shift and second-order quadrupolar shift

In Fig. 4, the two high-field $^{87}RbNO_3$ DAS peaks overlap in the 11.7 T MQMAS spectrum, as they do in a DAS spectrum taken at 7.0 T [14]. This overlap indicates that sites with different chemical shifts and quadrupolar interactions can appear at the same frequency in a DAS or MQMAS spectrum. Such an 'accidental' overlap is a result of the cancellation of the chemical shift difference and the second-order quadrupolar shift difference. For well crystallized samples this type of overlap can be overcome by multiple-field experiments. However, one can also perform both DAS and MQMAS experiments on the same sample at only one field, since the overlap conditions are different for these two experiments. In this respect, the combination of DAS and MQMAS removes the possibility of spectral misinterpretation.

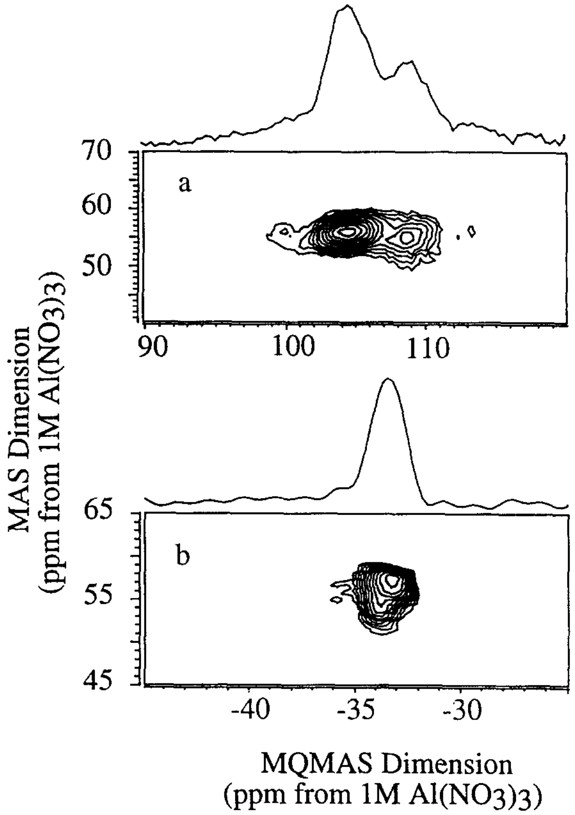

Fig. 5. 11.7T 3QMAS (a) and 5QMAS (b) ^{27}Al spectra of goosecreekite. Both spectra were acquired using the pulse sequence shown in Fig. 1(a).

For materials with a continuous distribution of chemical shifts and quadrupolar coupling constants (as in many amorphous and glassy materials), the problem of overlapping peaks limits the applicability of DAS and MQMAS. To see this, it is necessary to give a brief description of the general features of the DAS spectra for glassy materials. DAS spectra of these materials are broadened usually from one to twenty kilohertz by the distribution of chemical sites (which have a distribution of chemical shift and quadrupolar parameters) in these systems. Because DAS gives a two-dimensional spectrum correlating the isotropic DAS shifts and the anisotropic interactions, an anisotropic slice taken perpendicular to the DAS dimension corresponds to a VAS spectrum and can be simulated to provide a set of quadrupolar (C_Q and η_Q) and chemical shift (δ_{iso}) parameters [12,33]. These parameters are related to structural information such as the Si–O–Si bond angles for bridging oxygen in ^{17}O glass [12,33]. The above approach assumes that each slice that is taken out corresponds to only one type of site. Because it is possible that sites with different chemical environments show up at the same frequency, this assumption does not necessarily hold.

As an example, consider the amorphous $Si^{17}O_2$ DAS data obtained by Baltisberger et al. [33]. Using the quadrupolar and chemical shift parameters they obtained, the isotropic shifts in DAS, triple-quantum MAS and five-quantum MAS spectra were calculated using Eqs. (9) and (10). The results are shown in Fig. 6(a), where 100 ppm is first subtracted from the 5QMAS shifts and then plotted. The data points on the left side of the figure are characterized by substantial error bars, which is mainly a result of simulation errors. The observed DAS shifts change (increase) monotonically as a function of the slice number whereas the multiple quantum shifts do not vary monotonically over the corresponding slices. What is also noted is that the *spread* of MQMAS shifts is smaller for the same *sites* as in DAS as a result of the scaling factors in Eq. (9). For many of the ^{17}O inorganic glasses, the quadrupolar coupling constants (C_Q) decrease with the increase of the isotropic chemical shifts over a wide range of the Si–O–Si bond angles [12,33]. While the effect of the decreasing C_Q is to shift the MQMAS spectra to higher frequency (more positive ppm values), this effect is partially undone by the simultaneous increase of the isotropic chemical shift (note the negative sign for k_1). The net result is a smaller spread of shifts in MQMAS spectra of ^{17}O glasses than one would get from a similar DAS experiment. The reason for the difference between DAS and MQMAS is that k_1 and k_2 in DAS have the same sign (both are +1), but they have opposite signs in MQMAS.

While Fig. 6(a) shows that glassy samples may have a potential problem with overlap, it is worth considering a crystalline ^{17}O sample. Fig. 6(b) shows similar calculations for the five ^{17}O sites in well crystallized coesite [34]. All five sites are clearly separated in DAS, but sites 3, 4, and 5 are expected to overlap in the 3QMAS spectrum, and sites 4 and 5 are expected to overlap in the 5QMAS spectrum. This sort of overlap is possible in any sample depending on the relative sizes of the coupling constants and shifts. In this regard, performing all three experiments (DAS, 3QMAS and 5QMAS) would provide useful overall information as the overlap conditions for these techniques are different.

4.5. Sideband pattern

A 2D slow-spinning ($\omega_r = 3.4$ kHz) MQMAS spectrum for $^{23}Na_2C_2O_4$ is shown in Fig. 7. The sidebands in each slice shown to the right of the contour plot are separated from each other by 1.9 kHz, instead of 3.4 kHz. Also, the center-band and sideband positions in different slices taken along the isotropic MQMAS dimension are not the same.

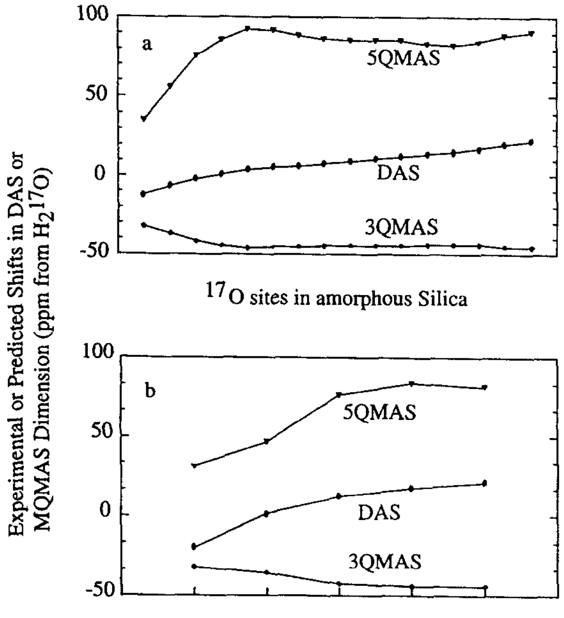

^{17}O sites in amorphous Silica

Five ^{17}O sites in Coesite

Fig. 6. Comparison of the resonance frequencies of DAS, 3QMAS and 5QMAS spectra for amorphous $Si^{17}O_2$ (a) and coesite (b). The Larmor frequency is 67.7 MHz corresponding to ^{17}O at 11.7 T. The isotropic chemical shift and quadrupolar coupling constant values are taken from [32,33], respectively. 100 ppm is first subtracted from the 5QMAS shifts and then plotted in the figure.

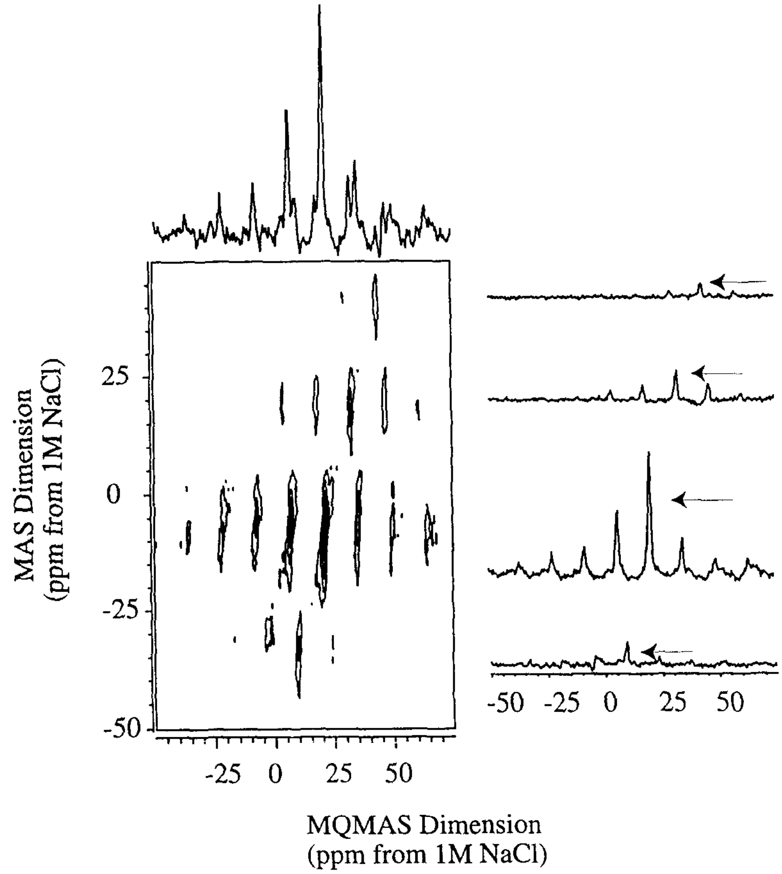

Fig. 7. MQMAS sideband pattern for ^{23}Na in $Na_2C_2O_4$ at 11.7 T. The spinning speed is 3.4 kHz and the sidebands in each of the isotropic slices are separated by $\omega_r/(1+k) = 1.9$ kHz. The arrows point to the center bands in the MQMAS dimension. Notice that they are not at the same positions due to the shearing transformation. Adding these sidebands together gives the projection shown above the contour plot with reduced resolution.

This can be seen in Fig. 7, where the arrows point to the center-band positions in different slices. The projection above the contour-plot shows lower resolution than the slices due to the overlap of different sidebands.

This complicated sideband pattern is a result of the redefinition of the t_1 dimension dwell time and the shearing transformation [35]. As the evolution time in the MQMAS dimension is divided into two parts, the dwell time in this dimension is redefined as:

$$DW_{\mathrm{iso}} = (k+1)DW_1 \qquad (11)$$

where DW_1 is the time increment in the t_1 dimension and k is defined in Eq. (6). The scaling of the dwell time causes the sidebands in this dimension to be separated from each other by integer multiples of the scaled spinning speed $\omega_r/(1+k)$. In this respect, the 'virtual' spinning speed in an isotropic slice is $0.56\omega_r$ or $0.39\omega_r$ for $I = 3/2$ or $5/2$ nuclei (Table 1), which agrees with the result in Fig. 7, where the sidebands are separated from each other by 1.9 kHz ($0.56\omega_r$).

To understand the complicated 2D sideband pattern fully, we use a pair of integers (m,n) to specify each sideband in the 2D spectrum where m denotes the MAS dimension sideband order, and n denotes the MQMAS dimension sideband order. Due to the shearing transformation [22,23,35] applied to achieve high resolution, the (m,n) sideband in the isotropic slice is $(m\frac{k}{1+k} + n\frac{1}{1+k})\omega_r$(kHz) away from the center band ($m = 0$, $n = 0$). This gives lower resolution when a projection is performed since sidebands corresponding to different (m,n) pairs overlap. In this case, a projection of only the $m = 0$ sidebands results in better resolution. An alternative way to accomplish the projection is first to shift the positions of the sidebands with $m \neq 0$ and then to perform the projection.

It is also worth noting that DAS spectra with similar sideband features have been described elsewhere [35]. The similarity is not surprising as DAS and MQMAS use similar 2D schemes to achieve high resolution. Another example of a complicated sideband pattern is shown in Fig. 8 for $^{87}Rb_2CrO_4$, where the sidebands arise primarily from the CSA.

A distinct feature in Fig. 7 is the existence of more spinning sidebands in the isotropic dimension than in the MAS dimension. This is a result of the

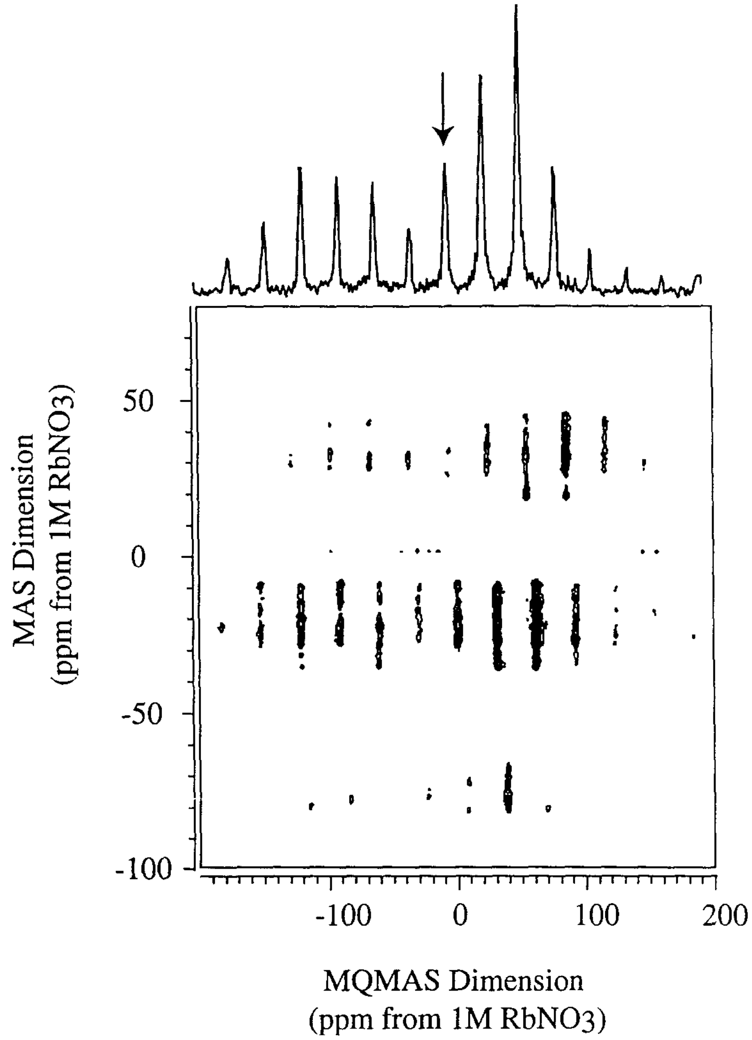

Fig. 8. 11.7 T MQMAS spectrum for ^{87}Rb in Rb_2CrO_4. The contour lines are drawn from a level of 10% to a level of 100% with an increment of 4.7%. The projection of the center band is shown above the contour plot. Due to the phase distortion, a magnitude spectrum is shown and the arrow points to the center band. The number of points in both dimensions is 512. The t_1 increment is 5 μs between two consecutive slices, and the t_2 dimension dwell time is 10 μs. 192 FIDs were accumulated for each t_1 point with a recycle delay of 0.5 s giving a total acquisition time of 28 h.

CSA for ^{23}Na, which is magnified by a factor of three for the triple-quantum coherence and results in more sidebands in the isotropic dimension (but no additional MAS dimension sidebands). An enhancement of the sideband intensity was also observed for ^{45}Sc in $Li_3Sc_2(PO_4)_3$, but in this case it was due to the magnified second-order quadrupolar effect instead of the CSA. Such an effect is about 2.3 times larger for the triple-quantum coherence than for the single-quantum coherence (see Table 1, C_1s and C_2s for $I = 7/2$ nuclei), again resulting in the additional sidebands in the isotropic dimension.

4.6. Chemical shift anisotropy

As discussed in Section 2 of this paper, the CSA effect is magnified by a factor of $m \rightarrow -m$ for the transition, which allows it to dominate the triple-quantum spectrum when its magnitude is comparable to that of the second-order quadrupolar interaction in the single-quantum spectrum. Simulation of the MQMAS spectrum then directly yields the CSA parameters. The validity of this approach is also based on the fact that the magnitude of the second-order quadrupolar interaction for the triple-quantum coherence of a spin 3/2 nucleus is scaled by a factor of 7/9, compared with that for the single quantum coherence under MAS (see Table 1, C_2 for $I = 3/2$ nuclei).

Figs. 8 and 9(a) show the 11.7 T ^{87}Rb MQMAS ($\omega_r = 8.9$ kHz) and DAS spectra, respectively, of Rb_2CrO_4. Two sites exist in this compound [14,36], but only the one with smaller C_Q was observed in both experiments. The CSA and the second-order quadrupolar broadening at 11.7 T are ~ 27 kHz ($\delta_{cs} = -110$ ppm) and ~ 13 kHz ($C_Q = 3.5$ MHz), respectively [37]. Since the combined effect of the CSA and quadrupolar interactions is complicated, the DAS and MAS spectra are not sensitive to variations in the CSA parameters. It is then very difficult to obtain CSA information from either the DAS or MAS spectra. However, as the CSA is amplified to ~ 75 kHz in the MQMAS dimension, the MQMAS spectrum of Rb_2CrO_4 covers a much larger frequency range and has more spinning sidebands. It is thus possible to neglect the second-order quadrupolar effect when we simulate the MQMAS sideband intensities. The simulated spectrum is shown in Fig. 8(c) and the magnitude of the CSA, together with the asymmetry parameter can be determined ($\delta_{cs} = -110$ ppm, $\eta_{cs} = 0.0$). These values are in good agreement with those determined by a switching angle spinning (SAS) approach [37] but do not agree with other numbers found in the literature [36]. The Rb_2CrO_4 spectrum here also serves as an example to demonstrate that relatively large CSA does not limit the implementation of the MQMAS.

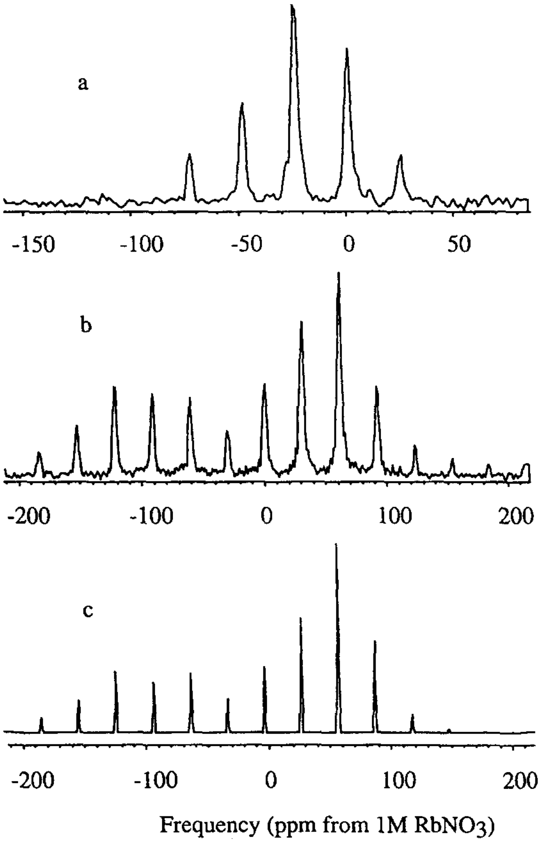

Fig. 9. (a) 11.7 T DAS spectrum for ^{87}Rb in Rb_2CrO_4, (b) 11.7 T MQMAS spectrum for ^{87}Rb in Rb_2CrO_4, (c) Simulated MQMAS spectrum with $\delta_{cs} = -110$ ppm, $\eta_{cs} = 0.0$. The simulation includes only the CSA effect, neglecting the second-order quadrupolar effect.

4.7. MQVAS

As we have shown in Section 2, CSA information can also be derived by performing the triple-quantum experiment at 70.12° or 30.56° and removing the second-order quadrupolar effect by a correlation scheme. Additionally, because the CSA is magnified by a factor of three in the triple-quantum dimension compared with the single-quantum dimension, this approach would have the advantage of allowing one to obtain CSA parameters even if the CSA is too small to show significant effects on the single-quantum spectrum. Experimentally, this can be realized using the same sequence as in Fig. 1.

Fig. 10 shows the 11.7 T $RbNO_3$ MQVAS spectrum acquired with the sample spinning at 70.12°. Three sites exist in the salt, and the isotropic chemical shifts and quadrupolar parameters for each site have been determined from DAS and MQMAS [23]: $\delta_{iso} = -27.4$ ppm, $C_Q = 1.68$ MHz, $\eta_Q = 0.2$ for the first site, $\delta_{iso} = -28.5$ ppm, $C_Q = 1.94$ MHz, $\eta_Q = 1.0$ for the second and $\delta_{iso} = -31.3$ ppm, $C_Q = 1.72$ MHz, $\eta_Q = 0.5$ for the third. Using these parameters, the isotropic frequency shifts in the triple-quantum dimension were calculated to give -74.2, -71.4 and -84.9 ppm, respectively, for the three sites. These numbers are in the same region as the peaks in the triple-quantum spectrum. Compared with the simulations in Fig. 11, it is likely that the spectrum shows well-defined patterns for different sites. However, accurate determination of the CSA parameters for this salt requires a three-dimensional experiment to separate the different resonances.

We have recorded pure-absorption mode MQVAS spectra for ^{23}Na and ^{87}Rb in several other compounds ($^{23}Na_2C_2O_4$, $^{23}Na_2SO_4$, $^{87}RbClO_4$, $^{87}Rb_2SO_4$). All of the triple-quantum spectra show asymmetric peaks, but no clear singularities can be identified to accurately determine the CSA parameters, most likely due to the existence of other anisotropic interactions such as dipolar coupling. The possibility that other interactions might obscure the triple-quantum spectra suggests that MQVAS can be

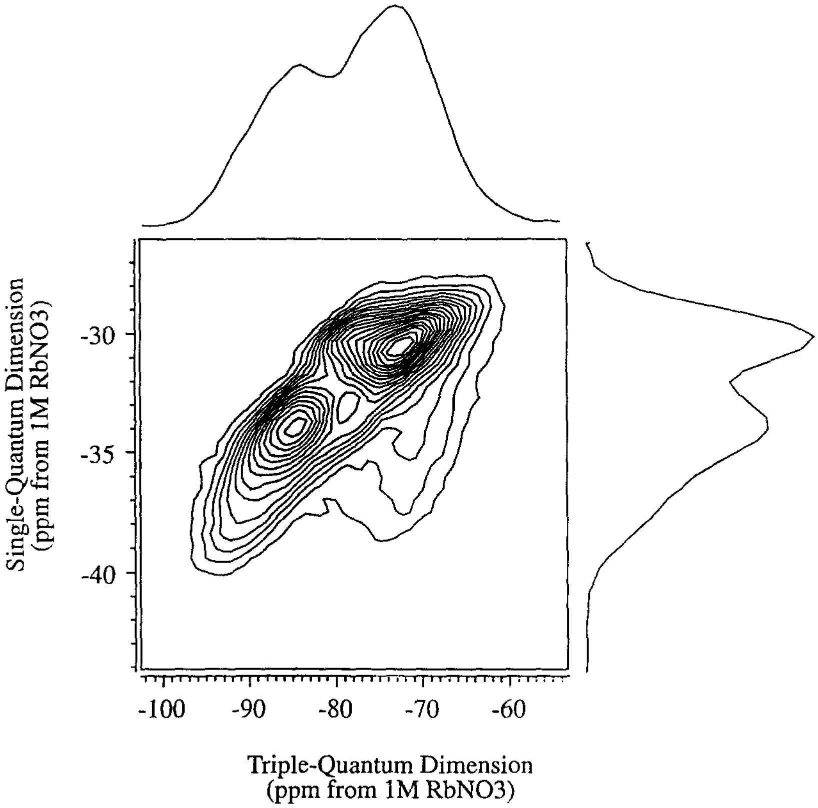

Fig. 10. 11.7 T MQVAS spectrum for ^{87}Rb in $RbNO_3$. 128 t_1 points and 512 t_2 points were collected. 192 FIDs were accumulated for each t_1 point with a recycle delay of 0.5 s giving a total acquisition time of 7 h.

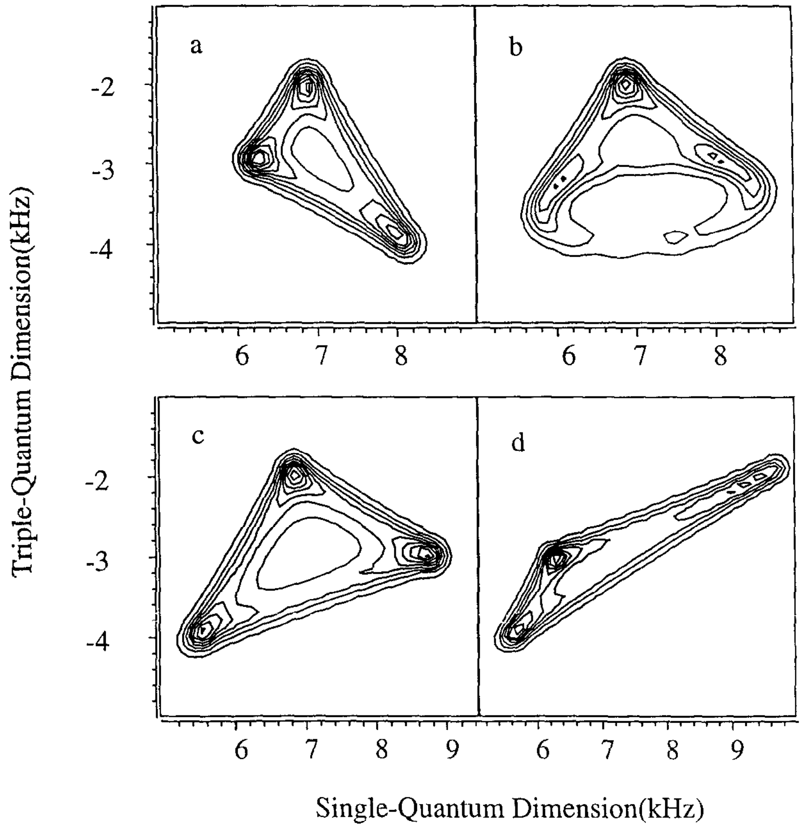

Fig. 11. Simulated two-dimensional MQVAS patterns with different Euler angles. The parameters used for the simulations are: $C_Q = 3.0\,\text{MHz}$, $\eta_Q = 1.0$, $\delta_{iso} = 0\,\text{ppm}$, $\delta_{cs} = 15\,\text{ppm}$, $\eta_{cs} = 1.0$, $I = 3/2$, and the Larmor frequency is 150 MHz. The Euler angles are (a) (0°,0°,0°) (b) (0°,0°,45°) (c) (0°,0°,90°) (d) (90°,90°,90°).

useful only when the CSA is moderate, e.g., when it is large enough to dominate the triple-quantum dimension, but not larger than the spinning speed.

Recently, it was shown that the 2D switching-angle spinning (SAS) spectra for quadrupolar nuclei are more sensitive to the relative orientation (described by a set of Euler angles α, β, and γ between the CSA and quadrupolar principal axes) than the 1D MAS or static spectra [37]. To see how these angles could affect the MQVAS spectra, Fig. 11 shows our simulated 2D MQVAS spectra using the same chemical shift and quadrupolar parameters but different sets of Euler angles. As in the SAS spectra, these patterns show a significant dependence on the relative orientation of the two tensors, providing a promising method for quantifying these angles. One feature of the two-dimensional pattern is that although the 1D projection does not always show clear singularities, the two-dimensional pattern often does [37,38]. This was verified by several MQVAS spectra and a complete analysis of these patterns is under way.

5. Conclusion

The complimentary aspects of MQMAS and DAS have been studied. By examples, we have shown that the technically simple MQMAS technique is suitable for the study of ^{23}Na and ^{87}Rb with some care necessary for site quantification; for nuclei such as ^{27}Al, ^{11}B and ^{45}Sc, MQMAS spectra are useful even when DAS fails to provide high-resolution spectra; due to 'accidental overlap' of different resonances, performing both the MQMAS and DAS experiments can be useful in qualification because the spectra overlap differently.

In addition, we have also studied some aspects of the MQMAS technique including the linewidth and resolution, the sideband pattern and the effect of CSA and dipolar interactions on the resultant spectra. Two extensions of MQMAS have also demonstrated that CSA information can be directly obtained using the multiple-quantum scheme.

With the line-narrowing techniques developed for quadrupolar nuclei, it is now possible to study a variety of important quadrupolar nuclei such as ^{17}O, ^{27}Al, ^{11}B, ^{23}Na, ^{85,87}Rb, ^{69,71}Ga and ^{45}Sc in solids. A combination of these averaging schemes with other NMR techniques could result in more advanced approaches for the investigation of quadrupolar systems. For example, the combination of DAS or MQMAS with HETCOR (hetero-nuclear correlation) have yielded high-resolution HETCOR spectra for quadrupolar nuclei [39,40]; the introduction of the SAS or MQVAS schemes could lead to a complete separation of resonance lines and a determination of the quadrupolar and CSA tensors for each of the distinct sites in the material.

Acknowledgements

We would like to thank Dr. J.S. Shore, M. Ernst, and Y. Lin for helpful discussions. We also thank to Dr. L. Frydman for sending us the preprint of Ref. [15] and Dr. P.J. Grandinetti for Ref. [23]. M. Augustine and S. Depaul are thanked for carefully reading the manuscript. The authors would like to thank J.C. Gabriel, W.S. Wise, and J.R. Boles for providing a purified sample of goosecreekite. This work was supported by the Director, Office of Energy Research, Office of Basic Energy Sciences, Materials Sciences Division of the US Department of Energy under Contract No. DE-AC03-76SF00098, and by NSF grant number EAR 9506393 to J.F. Stebbins. J.H.B. was partially supported by a Camille and Henry Dreyfus Start-up grant and a Research Corporation Cottrell College Grant.

References

[1] E.R. Andrew, A. Bradbury, and R.G. Eades, Nature, 182 (1958) 1659.
[2] E.R. Andrew, A. Bradbury, and R.G. Eades, Nature, 183 (1959) 1802.
[3] I.J. Lowe, Phys. Rev. Lett., 2 (1959) 285.
[4] A. Samoson, E. Kundla, and E. Lippmaa, J. Magn. Reson., 49 (1982) 350.
[5] S. Schramm and E. Oldfield, J. Am. Chem. Soc., 106 (1984) 2502.
[6] A. Samoson, E. Lippmaa, and A. Pines, Mol. Phys., 65 (1988) 1013.
[7] Y. Wu, B.Q. Sun, and A. Pines, J. Magn. Reson., 89 (1990) 297.
[8] B.F. Chmelka and J.W. Zwanziger, in NMR Basic Principles and Progress, Vol. 33, Springer, Berlin, Heidelberg, 1994.
[9] K.T. Mueller, B.Q. Sun, G.C. Chingas, J.W. Zwanziger, T. Terao, and A. Pines, J. Magn. Reson., 86 (1990) 470.
[10] A. Llor and J. Virlet, Chem. Phys. Lett., 152 (1988) 248.
[11] K.T. Mueller, Y. Wu, B.F. Chmelka, J. Stebbins, and A. Pines, J. Am. Chem. Soc., 113 (1991) 32.
[12] I. Farnan, P.J. Grandinetti, J.H. Baltisberger, J.F. Stebbins, U. Werner, M.A. Eastman, and A. Pines, Nature, 358 (1992) 31.
[13] Y. Wu, B.F. Chmelka, A. Pines, M.E. Davis, P.J. Grobet, and P.A. Jacobs, Nature, 346 (1990) 550.
[14] J.H. Baltisberger, S.L. Gann, E.W. Wooten, T.H. Chang, K.T. Mueller, and A. Pines, J. Am. Chem. Soc., 114 (1992) 7489.
[15] L. Frydman and J.S. Harwood, J. Am. Chem. Soc., 117 (1995) 5367.
[16] A. Medek, J.S. Harwood, and L. Frydman, J. Am. Chem. Soc., 117 (1995) 12779.
[17] S. Vega, J. Chem. Phys., 68 (1978) 5518.
[18] L. Emsley and A. Pines, in B. Maraviglia (Ed.), Lectures on Pulsed NMR, 2nd edn., Societa Italiana di Fisica, 1994, p. 1.
[19] J.P. Amoureux, Solid State NMR, 2 (1993) 83.
[20] J.H. Baltisberger, Z. Xu, J.F. Stebbins, S.H. Wang, and A. Pines, J. Am. Chem. Soc., 118 (1996) 7209.
[21] M.A. Eastman, P.J. Grandinetti, Y.K. Lee, and A. Pines, J. Magn. Reson., 98 (1992) 333.
[22] P.J. Grandinetti, J.H. Baltisberger, A. Llor, Y.K. Lee, U. Werner, M.A. Eastman, and A. Pines, J. Magn. Reson., 103 (1993) 72.
[23] D. Massiot, B. Touzo, D. Trumeau, J.P. Courtures, J. Virlet, P. Florian, and P.J. Grandinetti, Solid State NMR, 6 (1996) 73.
[24] C. Fernandez and J.P. Amoureux, Solid State NMR, 5 (1996) 315.
[25] C. Fernandez, J.P. Amoureux, L. Delmotte, Y. Dumazy, and L. Delevoye, Proc. 37th Experimental Nuclear Magnetic Resonance Conf., Pacific Grove, California, March 1996, p. 217.
[26] J.F. Stebbins, in T.J. Ahrens (Ed.), Nuclear Magnetic Resonance Spectroscopy of Silicates and Oxides in Geochemistry

and Geophysics, American Geophysical Union, Washington DC, 1995, p. 303.

[27] J.H. Baltisberger, S.L. Gann, P.J. Grandinetti, and A. Pines, Mol. Phys., 81 (1994) 1109.

[28] D. Massiot, I. Farnan, N. Gauthier, D. Trumeau, P. Florian, and P.J. Grandinetti, Proc. 36th Experimental Nuclear Magnetic Resonance Conference, Boston, Massachusetts, March 1995, p. 465.

[29] D. Freude and J. Haase, in NMR Basic Principles and Progress, Vol. 29, Springer, Berlin, Heidelberg, 1993, p. 1.

[30] K.T. Mueller, G.C. Chingas, and A. Pines, Rev. Sci. Instrum., 62 (1991) 1445.

[31] C. Fernandez and J.P. Amoureux, Chem. Phys. Lett., 242 (1995) 449.

[32] R.C. Rouse and D.R. Peacor, Am. Mineral., 71 (1986) 1494.

[33] J.H. Baltisberger, Thesis, University of California, Berkeley, 1993.

[34] P.J. Grandinetti, J.H. Baltisberger, I. Farnan, J.F. Stebbins, U. Werner, and A. Pines, J. Phys. Chem., 99 (1995) 12341.

[35] P.J. Grandinetti, Y.K. Lee, J.H. Baltisberger, B.Q. Sun, and A. Pines, J. Magn. Reson., 102 (1993) 195.

[36] J.T. Cheng, J.C. Edwards, and P.D. Ellis, J. Phys. Chem., 94 (1990) 553.

[37] J.S. Shore, S.H. Wang, R.E. Taylor, A.T. Bell, and A. Pines, J. Chem. Phys., submitted for publication.

[38] M. Linder, A. Hohener, and R.R. Ernst, J. Chem. Phys., 73 (1980) 4959.

[39] T.P. Jarvie, R.M. Wenslow, and K.T. Mueller, J. Am. Chem. Soc., 117 (1995) 570.

[40] L.M. Bull, S.H. Wang, S. Depaul, and A. Pines, J. Magn. Reson., submitted for publication.